

# Encoding high-order cylindrically polarized light beams

Ignacio Moreno,<sup>1,\*</sup> Jeffrey A. Davis,<sup>2</sup> Don M. Cottrell,<sup>2</sup> and Ramiro Donoso<sup>3</sup>

<sup>1</sup>Departamento de Ciencia de Materiales, Óptica y Tecnología Electrónica, Universidad Miguel Hernández de Elche, 03202 Elche, Spain

<sup>2</sup>Department of Physics, San Diego State University, San Diego, California 92182-1233, USA

<sup>3</sup>Departamento de Ciencias Físicas, Universidad de La Frontera, Temuco, Chile

\*Corresponding author: i.moreno@umh.es

Received 11 June 2014; accepted 14 July 2014;  
posted 18 July 2014 (Doc. ID 213715); published 18 August 2014

In this work we present a setup for the experimental production of cylindrically polarized beams, as well as other variations of polarized light beams. The optical system uses a single transmissive phase-only spatial light modulator, which is used to apply different spatial phase modulation to two output collinear *R* and *L* circularly polarized components. Different cylindrically polarized light beams can be obtained by applying different phase shifts to these two circularly polarized components. The system is very efficient since modulation is directly applied to the light beam (as opposed to other common methods operating in the first order of encoded diffraction gratings). Different variations to the cylindrically polarized light beams are also reported, obtained by adding linear or quadratic relative phase shifts between the two circular polarization components of the light beam. Experimental results are provided in all cases. © 2014 Optical Society of America

*OCIS codes:* (260.5430) Polarization; (230.5440) Polarization-selective devices; (260.6042) Singular optics.

<http://dx.doi.org/10.1364/AO.53.005493>

## 1. Introduction

The production of two-dimensional (2D) polarization patterns is interesting for different applications including polarization imaging [1], data encoding [2], and polarization multiplexing [3]. More recently, a renewed interest emerged in the field, particularly because of the ability to spatially control the state of polarization with liquid crystal spatial light modulators (LC-SLMs) [4,5]. The production of radially and azimuthally polarized beams [6] was especially relevant because of their particularly interesting properties when they are focused, and because of their relation with the orbital angular momentum of light [7]. These beams can be regarded as the superposition of two circularly polarized light beams

with opposite helicity (one left [L] circular polarization and the other right [R] circular polarization), and each one carrying a vortex (spiral phase) with charges  $\ell = \pm 1$  [8]. Cylindrically polarized vector beams [9] are a generalization of such polarized light beams, which show a polarization map with symmetry around the optical axis.

In recent years, a number of different methods and systems have been developed to create such 2D polarization patterns, including interferometric systems [10], specially designed subwavelength structures [11], radially patterned polarizers [12], liquid crystal devices with specially designed shaped electrodes [13,14], and inhomogeneous birefringent elements named *q*-plates [15]. For simplicity, we will concentrate here on those techniques that utilize SLMs [16–28], since they allow the greatest freedom. Of these, there appear to be two main classes.

One approach [16–18] is based on optical processing systems, where binary phase gratings are encoded onto a SLM. This grating creates, on the plus and minus first diffraction orders, two beams that are complex conjugates of each other. These two beams are filtered, and their polarization states are modified in a proper different manner. Then, when recombined, they create the polarization vector beam. Another related approach was proposed in [19], where a grating computer-generated hologram is displayed onto a SLM within a Sagnac interferometer. These systems are limited by the fact that the two beams must be complex conjugates of each other. Additionally, the diffraction efficiency and the available space bandwidth are limited by the requirement of adding gratings to encode the phase information.

Another general approach for creating spatial polarization distributions is based on independently controlling two linear orthogonal polarization states either with different halves of a SLM [20–25] or with two different SLMs [26–28]. The approaches differ either in the type (reflective or transmissive) of SLM and the optical architecture used to split and/or combine the two independently modulated orthogonal polarized beams. Nevertheless, the capability to separately encode unrelated patterns gives these systems much greater flexibility.

In this work we present a variation on our previously reported system [22] that demonstrated complete control of the amplitude, phase, and polarization of a light beam by means of a single transmissive LC-SLM. In that prior work, our emphasis was on diffractive spatially variant patterns that act as polarization sensitive computer-generated holograms. This was achieved by independently modulating two orthogonal linear polarization components. In this present paper, we now modify that optical architecture to adapt it for the independent modulation of the two circular polarization components of the input beam. Thus, it becomes useful for the generation and control of cylindrically polarized light beams.

The presented approach presents advantages compared to other methods in the literature. First, since the optical system is based on the direct modulation of the light beam polarization components, it avoids the use of gratings. Therefore, it provides a good use of the available space bandwidth provided by the SLM, and it is highly efficient, since no filtering is required. In addition, the two circular polarization components are independently modulated. This flexibility allows trying a variety of experiments to create different kinds of polarization maps by imposing different content on these two components.

The outline of the paper is as follows. After this introduction, in Section 2 we describe the optical system and provide details of the required optical components. Then in Section 3 we show how some well-known cylindrically polarized light beams (like first order radial or azimuthal polarization) can be created by the superposition of two circular

polarized beams emerging from the system. We apply the Jones matrix formalism to analyze different cases and provide a first set of experimental results verifying the theory. Then, in Section 4, we provide other kinds of polarized beams, including cylindrically polarized beams with higher-order topological charges, with different topological charge in each circular polarization component, and other polarized beams that carry relative linear or quadratic opposite phases. These last two cases are totally new, to our knowledge, and we show that they produce a bend and a twist, respectively, of the spatial polarization distribution obtained with regular cylindrically polarized light beams.

## 2. Experimental System to Produce Spatial Polarization Patterns

The key point for the production of general cylindrically polarized light beams is the fact that they can be composed as a linear combination of two homogeneously circular polarized light beams with opposite helicity and different spiral vortex charges (topological charges). For instance, radially and azimuthally polarized light beams are generated when adding or subtracting  $L$  and  $R$  circular polarizations with charges  $\ell_L = -1$  and  $\ell_R = +1$  [8]. Therefore, we must build an optical architecture capable of creating two circularly polarized light beams and add a different phase pattern to each one.

This requires the ability to modulate the two components of the electric field. This is not the case with LCDs, where only one linear polarization component (parallel to the LC director) is modulated. Therefore, parallel aligned LCDs cannot be directly applied for such a purpose.

Here we adapt the experimental setup already demonstrated in [22], which was designed to modulate two linear orthogonal polarization components. The optical architecture is sketched in Fig. 1. A linearly polarized light beam is launched onto a transmissive parallel-aligned LC-SLM, with the polarization direction at  $45^\circ$  with respect to the LC director axis (note that this polarization direction can be adjusted to create different electric field

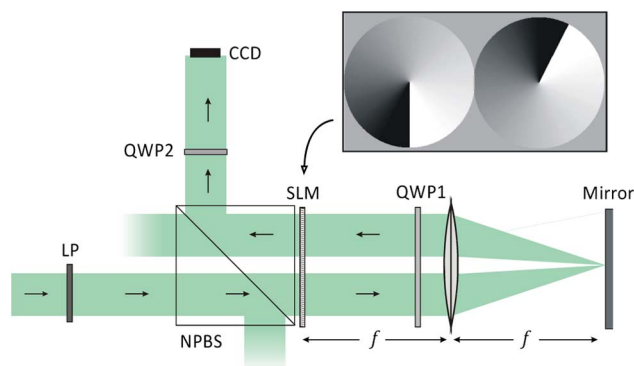


Fig. 1. Double pass system to generate the superposition of two circularly polarized beams with opposite helicity and different phase content.

strengths in the two orthogonal directions). This way the incoming beam is divided in two linear components with equal power, one parallel and another perpendicular to the LC director. While the first one is sensitive to the voltage applied to the display, the second one remains unaffected.

The system is based on dividing the SLM screen into two halves, where two different spiral phase patterns are addressed, as shown in Fig. 1. The initial beam illuminates only the left half of the SLM screen. The spiral phase pattern addressed on this part of the SLM is therefore encoded onto the vertical linear polarization component (the one parallel to the LC director). Then, by means of a lens and a mirror, the beam is reflected back to the right part of the SLM.

The insertion of the quarter-wave plate QWP1, located before the lens and oriented at 45° with respect to the LC director, produces a polarization change that reverses the orientation of initially vertical and horizontal linear polarization components. This way, the initial horizontal linear polarization component, which is not affected by the SLM in the first passage, now becomes polarized in the vertical direction on the beam impinging back on the right side of the SLM. Therefore, it will be modulated by the phase pattern encoded on this side of the SLM. In contrast, the initial vertical linear polarization component, which carries the phase pattern encoded on the first passage through the SLM, now becomes polarized in the horizontal direction, and it is not affected by the SLM on this second passage.

A nonpolarizing beam splitter (NPBS) is placed to separate the reflected beam from the incident beam. This NPBS introduces losses since the beam is split twice, and its use could be avoided by using a mirror. However, we have enough light power, and this way the system is compact. Therefore, the output beam reflected from the NPBS contains the superposition of two collinear beams with orthogonal linear polarizations and different phase encoded content. Note that Fig. 1 shows the encoding of different spiral phases on each side of the SLM. They might be different because we encode different topological charges or because we encode different phase offsets.

However, in order to effectively create the cylindrically polarized beams, the two emerging beams must be circularly polarized with opposite helicity. This is accomplished by placing a second quarter-wave plate (QWP2), again at 45° with respect to the LC-SLM director, at the NPBS exit. QWP2 transforms the vertical and horizontal linear polarizations onto *R* and *L* circular polarizations. Therefore, the collinear superposition of two *R* and *L* beams is obtained after QWP2, each one carrying different phase content introduced on each side of the SLM.

Note that this approach could be extended into a transformation of the vertical and horizontal linear polarizations into any two orthogonal elliptically polarized beams, either by using another orientation of QWP2 or by using a different retarder.

Next we present how by encoding different pairs of spiral phase patterns we can generate different cylindrically polarized light beams.

### 3. Production of Cylindrically Polarized Light Beams

We apply the Jones matrix formalism to analyze the combination of these two spiral circular polarized beams and how they produce such cylindrically polarized beams.

We begin with considering the superposition of two equally intense *L* and *R* circularly polarized light beams encoded with opposite spiral phases and phase offsets. The electric field of the beam emerging from QWP2 can be expressed as the following Jones vector:

$$\mathbf{E}(x, y) = \frac{1}{2} \begin{bmatrix} 1 \\ i \end{bmatrix} e^{+i(\ell\phi+\beta)} + \frac{1}{2} \begin{bmatrix} 1 \\ -i \end{bmatrix} e^{-i(\ell\phi+\beta)}. \quad (1)$$

Here  $\phi$  denotes the azimuthal coordinate;  $\ell$  is the vortex topological charge, which typically is an integer number (although fractional values might be also applied); and  $\beta$  is a phase offset that is applied to both circular polarizations. Therefore, each of the two circular polarization components carries an optical vortex, with opposite topological charges  $\pm\ell$ , and there is a phase shift  $2\beta$  among them.

This beam in Eq. (1) can be rewritten as

$$\mathbf{E}(x, y) = \frac{1}{2} \begin{bmatrix} e^{i(\ell\phi+\beta)} + e^{-i(\ell\phi+\beta)} \\ i(e^{i(\ell\phi+\beta)} - e^{-i(\ell\phi+\beta)}) \end{bmatrix} = \begin{bmatrix} \cos(\ell\phi + \beta) \\ \sin(\ell\phi + \beta) \end{bmatrix}. \quad (2)$$

Now we can generate various kinds of cylindrically polarized light beams simply by varying the order  $\ell$  encoded onto the spiral phases and the phase shift  $2\beta$  between the components. For example, if  $\beta = 0$ , then we form radially polarized light beams as

$$\mathbf{E}_{\text{rad}} = \begin{bmatrix} \cos(\ell\phi) \\ \sin(\ell\phi) \end{bmatrix}. \quad (3)$$

Alternatively, if we encode  $\beta = \pm\pi/2$ , then we get azimuthally polarized light beams as

$$\mathbf{E}_{\text{azi}} = \begin{bmatrix} \pm \sin(\ell\phi) \\ \cos(\ell\phi) \end{bmatrix}, \quad (4)$$

where the sign determines the sense of rotation of the polarization.

Other variants of the cylindrically polarized light are obtained either as a function of the charge  $\ell$  or as a function of the phase offset  $\beta$ .

The number  $\ell$  indicates the order of the cylindrically polarized light beam. While  $\ell = 1$  corresponds to the usual radial and azimuthal polarization, values  $|\ell| > 1$  provide higher-order cylindrically polarized light beams. The relative phase shift  $2\beta$  provides different polarization patterns for a given

order  $\ell$ . For instance, a spiral polarization beam is obtained for  $\ell = 1$  and  $\beta = \pm\pi/4$ .

To analyze these beams, we send them through a vertically oriented linear polarizer (defining vertical as the  $x$  direction). For the case of the cylindrically polarized light in Eq. (2) the resulting output Jones vector is given by

$$\begin{aligned} \mathbf{E}_{\text{out}}(x, y) &= \begin{bmatrix} 1 & 0 \\ 0 & 0 \end{bmatrix} \begin{bmatrix} \cos(\ell\phi + \beta) \\ \sin(\ell\phi + \beta) \end{bmatrix} \\ &= \cos(\ell\phi + \beta) \begin{bmatrix} 1 \\ 0 \end{bmatrix}; \end{aligned} \quad (5)$$

that is, it has an intensity of

$$I_{\text{out}}(x, y) = \cos^2(\ell\phi + \beta) = \frac{1}{2}[1 + \cos(2\ell\phi + 2\beta)]. \quad (6)$$

This shows a series of  $2\ell$  bright areas that can be rotated by adjusting the overall phase shift  $2\beta$ . If the analyzer is rotated by an angle  $\theta$ , the equation is modified as

$$I_{\text{out}}(x, y, \theta) = \frac{1}{2}[1 + \cos(2\ell\phi + 2\beta - \theta)]. \quad (7)$$

Figure 2 shows some experimental results obtained with the setup in Fig. 1, when  $\ell = 1$  is selected, for different values of the offset  $2\beta = 0, \pi/2, \pi$ , and  $3\pi/2$ . In these cases, first order cylindrically polarized beams are obtained. The corresponding polarization maps are drawn in each case.

For  $2\beta = 0$  and  $2\beta = \pi$  in Figs. 2(a) and 2(c), the well-known radial and azimuthal beams are obtained, respectively. In contrast, two orthogonal spiral polarization maps are obtained for  $2\beta = \pi/2$  and  $2\beta = 3\pi/2$  in Figs. 2(b) and 2(d), respectively. For each case, the expected polarization pattern is accompanied with experimental captures of the CCD camera, corresponding to the absence of final analyzer (experimental column in the left), and to the inclusion of an analyzer just before the CCD camera, oriented at  $\theta = 0^\circ, 45^\circ$ , and  $90^\circ$ , respectively.

The images without analyzer show a uniform pattern but include a dark point in the center that corresponds to the axial singularity created by the spiral phases. The polarization maps become clearly visible when the analyzer is included. The intensity patterns follow exactly the predictions of Eq. (7), showing a dark line, which defines the points where the polarization is orthogonal to the polarizer transmission axis. This dark line rotates as the analyzer rotates and also changes its initial position as  $\beta$  changes.

Note that, in all cases, the polarization state is fixed for a given value of the azimuth angle determined by the value of  $\beta$ . For instance, horizontal linear polarization is obtained along the horizontal axis for the radial polarization [Fig. 2(a)], while it is obtained at the vertical axis for the azimuthal polarization [Fig. 2(c)]. For the spiral polarization cases, horizontal linear polarization is obtained at  $\phi = \pm\pi/4$  and  $\phi = \pm3\pi/4$ , respectively [Figs. 2(b) and 2(d)]. This is opposed to other beams presented in the final section of this work, as we show later.

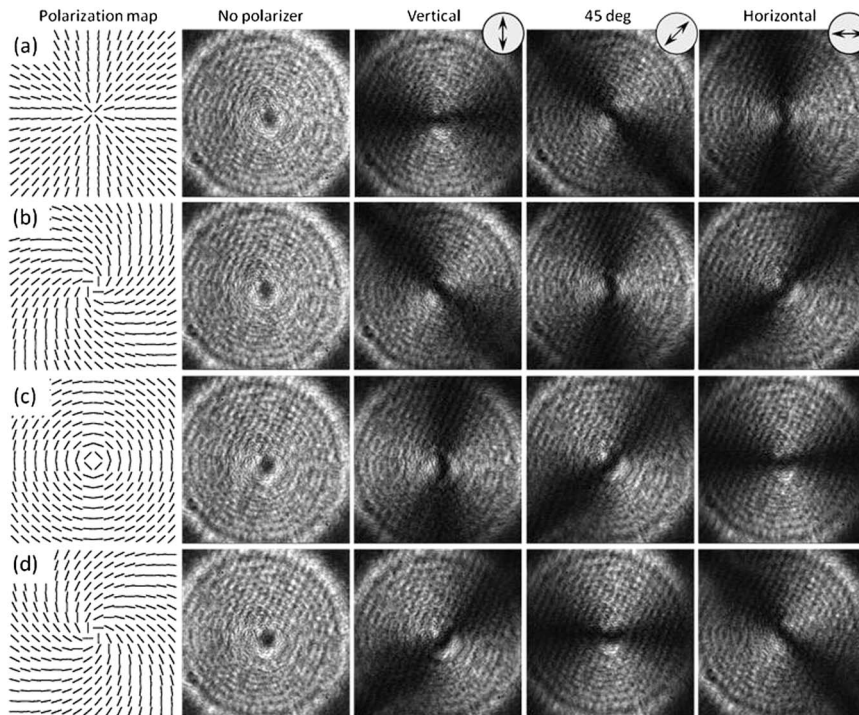


Fig. 2. Experimental realization of first order cylindrically polarized beams, obtained with  $\ell = 1$  and (a)  $2\beta = 0$ , radial polarization; (b)  $2\beta = \pi/2$ , spiral polarization; (c)  $2\beta = \pi$ , azimuthal polarization; and (d)  $2\beta = 3\pi/2$ , opposite spiral polarization.

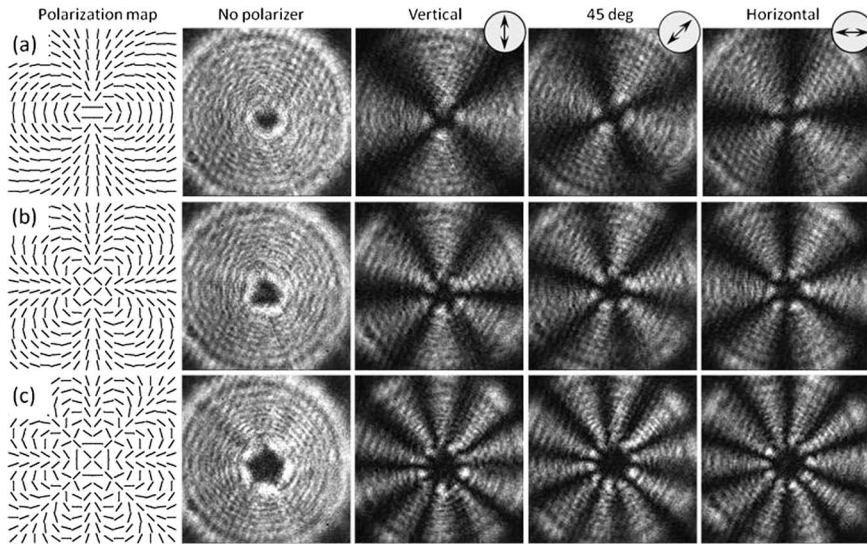


Fig. 3. Experimental realization of higher-order cylindrically polarized beams, obtained with  $\beta = 0$  and (a)  $\ell = 2$ , (b)  $\ell = 3$ , and (c)  $\ell = 5$ .

Higher-order cylindrically polarized light beams are obtained simply by encoding greater values of the topological charge  $\ell$ . As an example, in Fig. 3 we generated higher-order radially polarized beams, all obtained with  $\beta = 0$  but with topological charges  $\ell = 2, 3$ , and 5.

The expected polarization maps are drawn in the left column of Fig. 3 for each case. Now the polarization rotates faster versus the azimuth, due to the faster variations in the spiral phases encoded on each polarization component. Also note that as the topological charges are increased, so is the dark area in the center of the beam caused by the phase singularity.

When the analyzer is placed in front of the CCD camera, the intensity patterns that result again match very well with Eq. (7). In all cases, since  $\beta = 0$ , the linear polarization remains vertical along the spatial vertical line. This is why a bright vertical line is always obtained when the analyzer is oriented vertically. Then, the number of dark lines along the azimuthal angle is equal to  $2\ell$ . As before, the intensity pattern rotates as the analyzer rotates. Note that in all these cases again the polarization state is fixed at a given azimuth.

The extreme flexibility of this system allows adding multiple variations to these cylindrically polarized beams. Next we present some results where we generate other more exotic polarized beams.

#### 4. Other Polarized Light Beams

These previous results show the generation of cylindrically polarized beams with the superposition of the two circularly polarized components with the same topological charge and opposite sign. Note that in all these cases the spatial polarization distributions are symmetric with respect to a horizontal or vertical flip. Next we generate different polarized

beams by applying different content to the two circular components of the beam.

##### A. Polarized Beams with Different Charge on Each Circular Component

We start by considering two different spiral phases on each circular polarization component with topological charges  $\ell$  and  $m$ , respectively, and with  $\beta = 0$ . This allows the generation of other different polarized beams. Following the same treatment as in Eq. (1), we obtain the following superposition,

$$\mathbf{E} = \frac{1}{2} \begin{bmatrix} 1 \\ i \end{bmatrix} e^{+i\ell\phi} + \frac{1}{2} \begin{bmatrix} 1 \\ -i \end{bmatrix} e^{+im\phi}, \quad (8)$$

which can be rewritten as

$$\mathbf{E} = e^{+i\left(\frac{\ell+m}{2}\right)\phi} \begin{bmatrix} \cos\left[\left(\frac{\ell-m}{2}\right)\phi\right] \\ \sin\left[\left(\frac{\ell-m}{2}\right)\phi\right] \end{bmatrix}, \quad (9)$$

and the intensity transmitted by an analyzer which is vertically aligned is given by

$$I_{\text{out}} = \frac{1}{2} [1 + \cos((\ell - m)\phi)]. \quad (10)$$

The number of lobes is now determined by the difference of the two spiral phases. When  $m = -\ell$  the situation is analogous to that analyzed in the previous section, and the cylindrically polarized light beams are recovered. But with  $m \neq -\ell$ , different polarized beams can be generated.

Figure 4 shows some examples of this case. In Fig. 4(a) we selected  $\ell = 1, m = 0$ . As a result the polarization changes gradually in the beam, but with only a half cycle along the azimuthal direction. Therefore, polarization is linear and vertical along

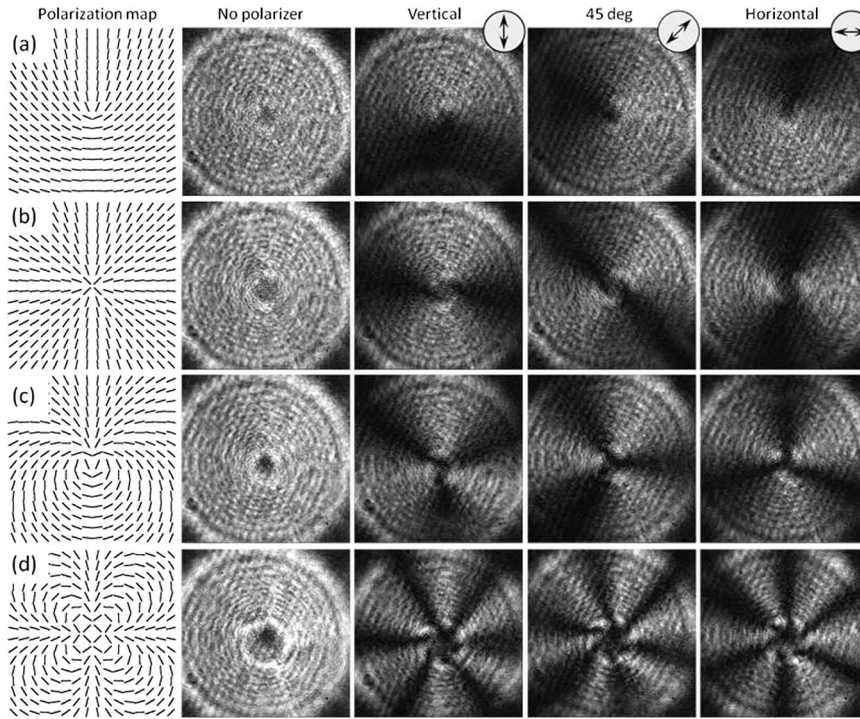


Fig. 4. Experimental realization of cylindrically polarized beams, obtained with  $\beta = 0$  and (a)  $\ell = 1, m = 0$ ; (b)  $\ell = 2, m = 0$ ; (c)  $\ell = 1, m = -2$ ; and (d)  $\ell = 1, m = -5$ .

the centered upper vertical line,  $\phi = 0$ , but becomes horizontal along the centered lower vertical line,  $\phi = \pi$ . As a result, when the analyzer is vertically oriented, the intensity gradually decreases along the azimuthal angle from top to bottom, in agreement with Eq. (10). Just like in the two previous cases in Figs. 2 and 3, the intensity pattern rotates as the orientation of the analyzer rotates.

Figure 4(b) shows another interesting case, where  $\ell = 2, m = 0$  were selected. In this case note that the same radial polarization pattern as in Fig. 2(a) is reproduced. Also the intensity patterns when the analyzer is included in the system are reproduced. However, there is a major difference between these two cases. Because one of the two circular components that constitute the polarized beam in Fig. 4(b) does not have the spiral phase, the axial singularity is not created for this beam. This is noticeable by regarding that the center of the beam is not perfectly dark, as it was the case in Fig. 2(a). This is the reason why we call this beam pseudo-radially polarized [29]. The phase difference between the pure radially polarized beam in Fig. 2(a) and this pseudo-radially polarized beam in Fig. 4(b) cannot be detected simply by regarding the intensity pattern, as we do here, but can be done by passing the beam through a vortex detecting grating [29].

Finally, the cases in Figs. 4(c) and 4(d) correspond to selecting  $\ell = 1, m = -2$  and  $\ell = 1, m = -5$ , respectively. Note that the number of dark lines along the azimuthal angle is equal to  $|\ell - m|$ , which in these cases are 3 and 6, respectively, in agreement with Eq. (10).

#### B. Applying a Linear Phase Shift

Now we can try some new ideas in order to generate some other polarized light beams that have not been reported earlier.

For this experiment, we use identical but opposite spiral phases and, as a novel feature, we also add opposite horizontal linear phases to each component. Consequently, the Jones vector is now written as

$$\mathbf{E} = \frac{1}{2} \begin{bmatrix} 1 \\ i \end{bmatrix} e^{i(\ell\phi + \gamma y)} + \frac{1}{2} \begin{bmatrix} 1 \\ -i \end{bmatrix} e^{i(-\ell\phi - \gamma y)}. \quad (11)$$

Here the parameter  $\gamma$  is the slope of the linear phases. Equation (11) can be rewritten as

$$\mathbf{E} = \begin{bmatrix} \cos(\ell\phi + \gamma y) \\ \sin(\ell\phi + \gamma y) \end{bmatrix}. \quad (12)$$

Therefore, note that now the Jones vector in Eq. (12) is controlled by two parameters: the topological charge  $\ell$  that provides the vortex but also the slope  $\gamma$  that adds an extra phase shift along the  $y$  direction.

For  $\gamma = 0$ , the regular radial polarized beams are retrieved. However, if  $\gamma \neq 0$ , an additional phase difference between the two electric field components is added, proportional to the  $y$  coordinate. This produces a distortion of the polarization map, which is modified and compresses the pattern toward the vertical direction.

Now, when this beam in Eq. (12) is launched onto a linear polarizer oriented in the vertical direction, the intensity at the output is given by

$$I_{\text{out}} = \frac{1}{2}[1 + \cos(2\ell\phi + 2\gamma y)]. \quad (13)$$

This now indicates that the number of lobes will change with  $y$  (horizontal coordinate)—increasing with smaller  $y$  and decreasing with larger  $y$ . This is shown in Fig. 5. Here, for simplicity, we have included the expected polarization map and only the corresponding experimental results with the vertically oriented analyzer polarizer. Cases with  $\ell = 1$  and  $\ell = 2$  are included. In both cases, three linear phases with slopes  $\gamma = \gamma_0, 2\gamma_0$ , and  $4\gamma_0$  are added.  $\gamma_0$  is an arbitrary constant value. We can see that the result is a bending of the dark lobes as the absolute value of the  $y$  coordinate increases, associated with a bending of the polarization directions in the polarization map. This bending increases with the slope of the linear phase.

For instance, in the most extreme case in Figs. 5(d) and 5(h), the linear polarization never reaches a horizontal orientation in the half lower of the beam. Thus, this area appears always bright. In contrast, dark lobes tend to concentrate on the upper half of the beam.

These types of polarized light beams have not been reported earlier, to our knowledge.

### C. Applying a Quadratic Phase Shift

Finally, we generated additional polarized beams by combining identical but opposite spiral phases and

additional but opposite quadratic phase shifts  $\exp(\pm i\delta r^2)$  to each  $R$  and  $L$  polarization component. Here  $\delta$  is a parameter that determines the strength of the quadratic phase, and  $r^2 = x^2 + y^2$  denotes the radial coordinate.

Consequently, following the same description as before, the Jones vector is written now as

$$\mathbf{E} = \begin{bmatrix} \cos(\ell\phi + \beta + \delta r^2) \\ \sin(\ell\phi + \beta + \delta r^2) \end{bmatrix}. \quad (14)$$

Now we send this Jones vector of light through a linear polarizer oriented in the vertical direction; the resulting intensity is given by

$$I_{\text{out}} = \frac{1}{2}[1 + \cos(2\ell\phi + 2\beta + 2\delta r^2)]. \quad (15)$$

This relation indicates that we get the same number of lobes along the azimuthal coordinate as with  $\delta = 0$ , but their location will depend on the radial coordinate. As a consequence, the lobes become twisted.

This is shown in Fig. 6. In Fig. 6(a) we start with the second order azimuthally polarized beam, which is obtained from Eq. (2) with  $\ell = 2$  and  $\beta = \pi/2$ . This beam, when analyzed with the vertically oriented polarizer, produces dark lines along horizontal and vertical axes.

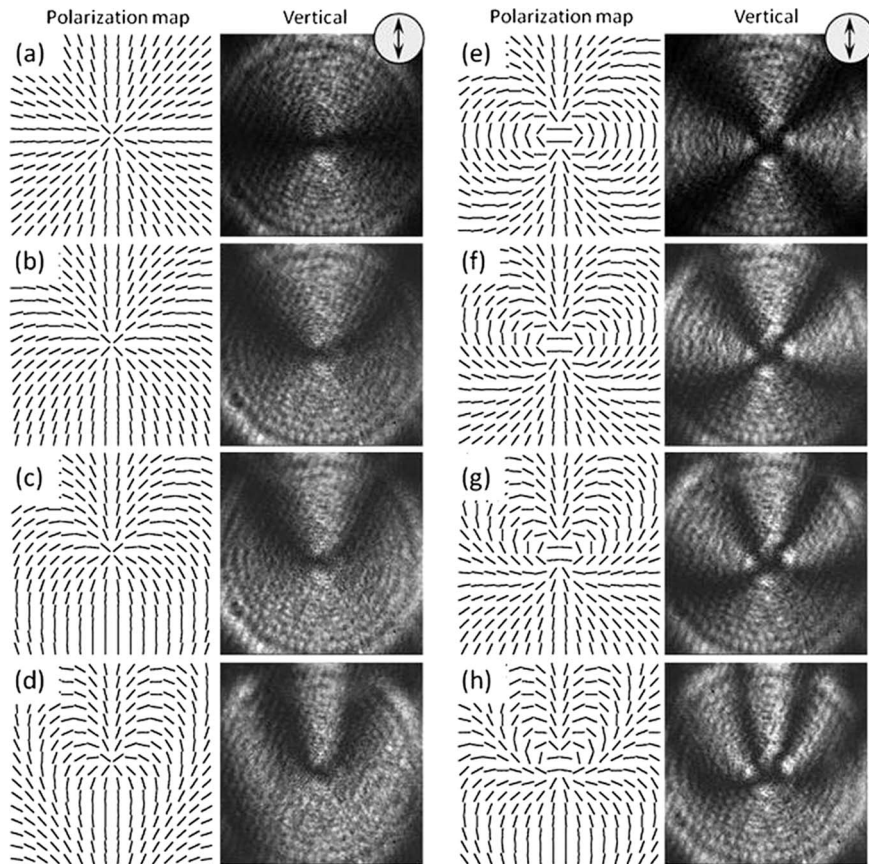


Fig. 5. Experimental realization of polarized beams obtained with  $\beta = 0$  and (a)–(d)  $\ell = 1$  and (e)–(h)  $\ell = 2$ , with additional linear phases with slope  $\gamma$  along the horizontal direction. (a) and (e)  $\gamma = 0$ ; (b) and (f)  $\gamma = \gamma_0$ ; (c) and (g)  $\gamma = 2\gamma_0$ ; (d) and (h)  $\gamma = 4\gamma_0$ .

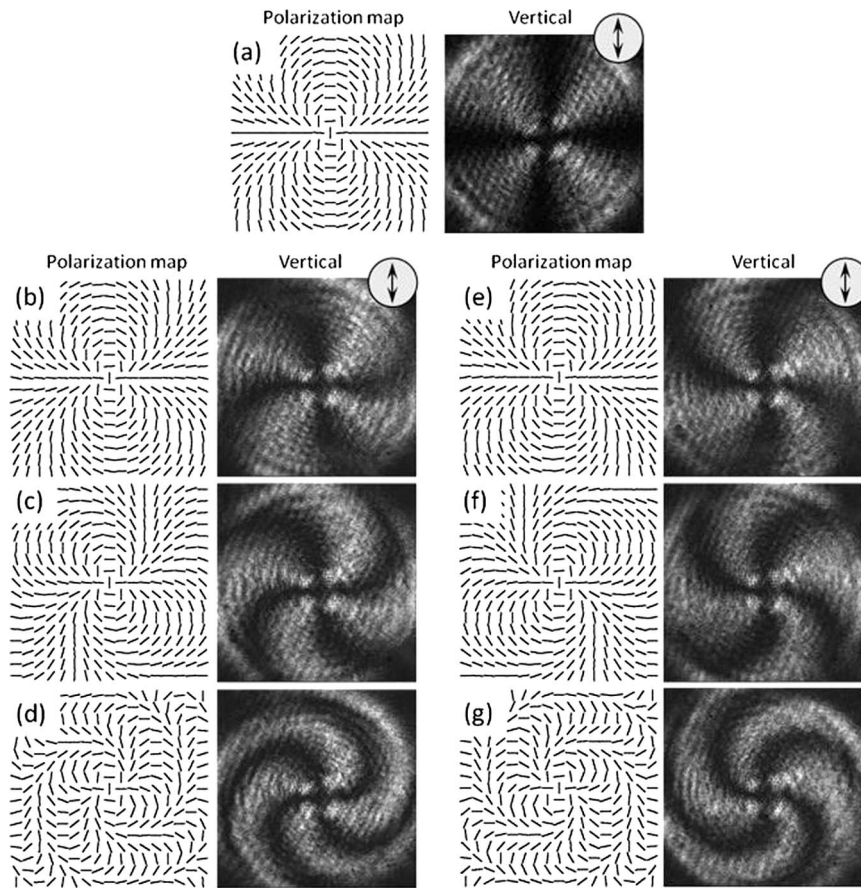


Fig. 6. Experimental realization of polarized beams with  $\beta = \pi/2$  and  $\ell = 2$ . (a)  $\delta = 0$ , (b)  $\delta = \delta_0$ , (c)  $\delta = 2\delta_0$ , (d)  $\delta = 4\delta_0$ , (e)  $\delta = -\delta_0$ , (f)  $\delta = -2\delta_0$ , (g)  $\delta = -4\delta_0$ .

Figures 6(b)–6(d) show the cases when a quadratic phase is added, with positive values  $\delta = \delta_0$ ,  $2\delta_0$ , and  $4\delta_0$ , respectively, while Figs. 6(e) and 6(f) correspond to the same negative values.  $\delta_0$  is again an arbitrary value. We can see how the dark lobes in Fig. 6(a) now become twisted, and the magnitude of the twist increases as the parameter  $\delta$  becomes greater. It is also noticeable how the sense of the lobes' twist is reversed when changing the sign of  $\delta_0$ .

## 5. Conclusions

In summary, we have presented results where we adapted a previously reported system designed to generate polarization computer-generated holograms [22] for the generation of cylindrically polarized light beams. The system is simple compared to others in the literature, and it is versatile because different phase patterns can be encoded onto the two  $R$  and  $L$  circular polarization components in order to produce different types of spatially polarized beams. In addition, this system is also very efficient since phase values are directly encoded by the phase of the liquid crystal display, without any codification requirement in terms of additional gratings and filtering operations.

We have first demonstrated the realization of regular first order ( $\ell = 1$ ) cylindrically polarized beams: radial, spiral, and azimuthal polarizations. Then,

higher-order ( $\ell > 1$ ) cylindrically polarized beams have been shown by encoding greater values of the topological charges encoded onto the  $R$  and  $L$  circular polarization components.

We finally generated some other more exotic polarized beams that show the great flexibility of the developed system. These have been obtained by adding different values of the topological charges in each polarization component or by adding additional opposite linear or quadratic phases. As a result, non-symmetric polarization patterns are obtained.

We expect that the simplicity of the proposed system and the great versatility that it provides will lead to more applications for these different polarized light beams.

I. Moreno and R. Donoso acknowledge financial support from Spanish Ministerio de Economía y Competitividad and FEDER Funds (Ref. FIS2012-39158-C02-02).

## References

1. J. E. Solomon, "Polarization imaging," *Appl. Opt.* **20**, 1537–1544 (1981).
2. A. V. Krishnamoorthy, F. Xu, J. E. Ford, and Y. Fainman, "Polarization-controlled multistage switch based on polarization-selective computer-generated holograms," *Appl. Opt.* **36**, 997–1010 (1997).
3. W. Yu, T. Konishi, T. Hamamoto, H. Toyota, T. Yotsuya, and Y. Ichioka, "Polarization-multiplexed diffractive optical

- elements fabricated by subwavelength structures," *Appl. Opt.* **41**, 96–100 (2002).
4. J. A. Davis, D. E. McNamara, D. M. Cottrell, and T. Sonehara, "Two-dimensional polarization encoding with a phase-only liquid-crystal spatial light modulator," *Appl. Opt.* **39**, 1549–1554 (2000).
  5. J. A. Davis, G. H. Evans, and I. Moreno, "Polarization-multiplexed diffractive optical elements with liquid-crystal displays," *Appl. Opt.* **44**, 4049–4052 (2005).
  6. S. Quabis, R. Dorn, M. Eberler, O. Glöckl, and G. Leuchs, "Focusing light into a tighter spot," *Opt. Commun.* **179**, 1–7 (2000).
  7. J. P. Torres, "Quantum engineering of light," *Opt. Pura Apl.* **44**, 309–314 (2011).
  8. I. Moreno, J. A. Davis, I. Ruiz, and D. M. Cottrell, "Decomposition of radially and azimuthally polarized beams using a circular-polarization and vortex-sensing diffraction grating," *Opt. Express* **18**, 7173–7183 (2010).
  9. Q. Zhan, "Cylindrical vector beams: from mathematical concepts to applications," *Adv. Opt. Photon.* **1**, 1–57 (2009).
  10. N. Passilly, R. de Saint Denis, K. Ait-Ameur, F. Treussart, R. Hierle, and J.-F. Roch, "Simple interferometric technique for generation of a radially polarized light beam," *J. Opt. Soc. Am. A* **22**, 984–991 (2005).
  11. Z. Bomzon, V. Kleiner, and E. Hasman, "Formation of radially and azimuthally polarized light using space-variant subwavelength metal stripe gratings," *Appl. Phys. Lett.* **79**, 1587–1589 (2001).
  12. I. Moreno, J. Albero, J. A. Davis, D. M. Cottrell, and J. B. Cushing, "Polarization manipulation of radially polarized beams," *Opt. Eng.* **51**, 128003 (2012).
  13. M. Stalder and M. Schadt, "Linearly polarized light with axial symmetry generated by liquid-crystal polarization converters," *Opt. Lett.* **21**, 1948–1950 (1996).
  14. J. Albero, P. Garcia-Martinez, N. Bennis, E. Oton, B. Cerrolaza, I. Moreno, and J. A. Davis, "Liquid crystal devices for the reconfigurable generation of optical vortices," *J. Light-wave Technol.* **30**, 3055–3060 (2012).
  15. F. Cardano, E. Karimi, S. Slussarenko, L. Marrucci, C. de Lisio, and E. Santamato, "Polarization pattern of vector vortex beams generated by q-plates with different topological charges," *Appl. Opt.* **51**, C1–C8 (2012).
  16. X.-L. Wang, J. Ding, W.-J. Ni, C.-S. Guo, and H.-T. Wang, "Generation of arbitrary vector beams with a spatial light modulator and a common path interferometric arrangement," *Opt. Lett.* **32**, 3549–3551 (2007).
  17. X.-L. Wang, Y. Li, J. Chen, C.-S. Guo, J. Ding, and H.-T. Wang, "A new type of vector fields with hybrid states of polarization," *Opt. Express* **18**, 10786–10795 (2010).
  18. J. Xin, C. Gao, C. Li, and Z. Wang, "Generation of polarization vortices with a Wollaston prism and an interferometric arrangement," *Appl. Opt.* **51**, 7094–7097 (2012).
  19. S. Liu, P. Li, T. Peng, and J. Zhao, "Generation of arbitrarily spatially variant polarization beams with trapezoid Sagnac interferometer," *Opt. Express* **20**, 21715–21721 (2012).
  20. C. Maurer, A. Jesacher, S. Fürhapter, S. Bernet, and M. Ritsch-Marte, "Tailoring of arbitrary optical vector beams," *New J. Phys.* **9**, 78 (2007).
  21. D. Preece, S. Keen, E. Botvinick, R. Bowman, M. Padgett, and J. Leach, "Independent polarisation control of multiple optical traps," *Opt. Express* **16**, 15897–15902 (2008).
  22. I. Moreno, J. A. Davis, T. Hernandez, D. M. Cottrell, and D. Sand, "Complete polarization control of light from a liquid crystal spatial light modulator," *Opt. Express* **20**, 364–376 (2012).
  23. W. Han, Y. Yang, W. Cheng, and Q. Zhan, "Vectorial optical field generator for the creation of arbitrarily complex fields," *Opt. Express* **21**, 20692–20706 (2013).
  24. J. H. Clegg and M. A. A. Neil, "Double pass, common path method for arbitrary polarization control using a ferroelectric liquid crystal spatial light modulator," *Opt. Lett.* **38**, 1043–1045 (2013).
  25. E. H. Waller and G. von Freymann, "Independent spatial intensity, phase and polarization distributions," *Opt. Express* **21**, 28167–28174 (2013).
  26. F. Kenny, D. Lara, O. G. Rodríguez-Herrera, and C. Dainty, "Complete polarization and phase control for focus-shaping in high-NA microscopy," *Opt. Express* **20**, 14015–14029 (2012).
  27. D. Maluenda, I. Juvells, R. Martínez-Herrero, and A. Carnicer, "Reconfigurable beams with arbitrary polarization and shape distributions at a given plane," *Opt. Express* **21**, 5432–5439 (2013).
  28. C.-S. Guo, Z.-Y. Rong, and S.-Z. Wang, "Double-channel vector spatial light modulator for generation of arbitrary complex vector beams," *Opt. Lett.* **39**, 386–389 (2014).
  29. J. A. Davis, D. M. Cottrell, B. C. Schoonover, J. B. Cushing, J. Albero, and I. Moreno, "Vortex sensing analysis of radially and pseudo-radially polarized beams," *Opt. Eng.* **52**, 050502 (2013).